IEEE Photonics Journal
An IEEE Photonics Society Publication

Open Access

High-Efficiency Ultra-Broadband Multi-Tip Edge Couplers for Integration of Distributed Feedback Laser With Silicon-on-Insulator Waveguide

Volume 11, Number 4, August 2019

Yi-Chou Tu
Po-Han Fu
Ding-Wei Huang

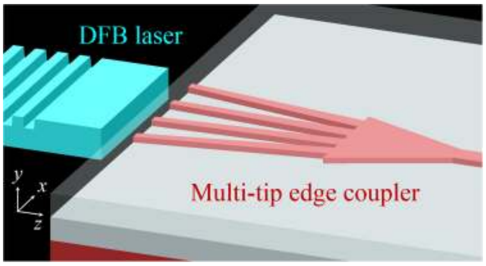

DOI: 10.1109/JPHOT.2019.2924477

High-Efficiency Ultra-Broadband Multi-Tip Edge Couplers for Integration of Distributed Feedback Laser With Silicon-on-Insulator Waveguide

Yi-Chou Tu,[1] **Po-Han Fu**,[1] **and Ding-Wei Huang** [1,2]

[1]Graduate Institute of Photonics and Optoelectronics, National Taiwan University, Taipei 10617, Taiwan
[2]Department of Electrical Engineering, National Taiwan University, Taipei 10617, Taiwan

DOI:10.1109/JPHOT.2019.2924477
This work is licensed under a Creative Commons Attribution 3.0 License. For more information, see https://creativecommons.org/licenses/by/3.0/

Manuscript received March 20, 2019; revised May 29, 2019; accepted June 19, 2019. Date of publication June 24, 2019; date of current version July 11, 2019. This work was supported by the Ministry of Science and Technology, Taiwan, R.O.C., under Grants 106-2221-E-002-140 and 107-2218-E-992-304. Corresponding author: Ding-Wei Huang (e-mail:dwhuang@ntu.edu.tw).

Abstract: A high-efficiency ultra-broadband multi-tip edge coupler based on a silicon-on-insulator platform for direct coupling with the elliptic beam of a distributed feedback laser was developed. The device is composed of a multi-tip section and a combiner section with extra offset regions to reduce the mode mismatch caused by the structural discontinuity which results from a limitation of the fabrication process that creates an inevitable gap width at the junction between the two sections. The widths and the spacing of the tips for the multi-tip section and the extra offset region for the combiner section are fine-tuned by using the particle swarm optimization method to reduce the mode mismatch. A high overall coupling efficiency up to 90.68% (0.4249 dB) at 1550 nm can be achieved for the optimized 90-μm-long four-tip edge coupler. The device can be operated over a broad spectral range of 1260–1675 nm with less than 1 dB extra loss. With its high-efficiency ultra-broadband operation and small device footprint, the proposed device is promising for laser-to-chip edge coupling in silicon photonics.

Index Terms: Diode lasers, waveguides, silicon nanophotonics, waveguide devices.

1. Introduction

The low absorption of typical telecommunication wavelengths and the high refractive index of silicon makes silicon-on-insulator (SOI) integrated photonics a promising platform for optical communication networks. Additionally, SOI integrated photonics can be compatible with complementary-metal-oxide-semiconductor (CMOS) manufacturing processes and large-scale photonic integration [1]–[3]. The coupling of a micrometer-scale light source and a few hundred-nanometer waveguide in silicon photonic integration for practical applications presents challenges due to the large mode mismatch and refractive index difference between the source and waveguide. Two types of structures have been developed to address these challenges and thus increase the coupling efficiency: the surface grating coupler and the edge coupler. The surface grating coupler is a periodic structure that diffracts the injected light at a specific angle and polarization into the waveguide modes [4]–[6]. However, it suffers from limited bandwidth and requires a complicated fabrication process to achieve a high coupling efficiency, e.g., a deposited silicon overlay with multi-step etching [5] or a multilayer reflector [6]. By contrast, the edge coupler is simply an inverse taper. Such a structure can expand the spatial distribution of the mode profile outside the waveguide core via shrinking the tip width [7], [8], leading to smaller mode mismatch between the laser source and the edge coupler. The structure can also reduce back reflection at the incident surface since the effective refractive index of SiO_2 is closer to that of air compared with Si. Additional advantages of edge couplers include a large bandwidth and low polarization-dependent loss [8].

The conventional edge coupler is composed of a single inverse taper with a rectangular waveguide cross section where the height of the waveguide core is typically fixed at 220 nm. In this arrangement, only the tip width can be adjusted to optimize the structure for greater mode match. Due to this limitation of the inverse taper design, the highest achievable coupling efficiency is limited. Several types of multi-tip edge couplers have been proposed so as to further reduce the coupling loss of conventional inverse taper edge couplers [9]–[12]. By varying the number, width and spacing between the tips, additional degrees of freedom are introduced to control the mode field distribution and thus enhance the coupling efficiency and improve the misalignment tolerances. The double-tip inverse taper with a multimode interference showed smaller coupling loss and an increased tolerance of misalignment than that of the single-tip coupler [9]. The three-tip waveguide with a double slot coupler has experimentally demonstrated a low insertion loss of 1.8 dB within a broad bandwidth for both transverse-electric (TE) and transverse-magnetic (TM) mode polarization [12].

So far, a majority of current publications have studied the coupling between the edge coupler and the circular beam from the lensed fiber or the small-core fiber with a mode field diameter (MFD) of 2.5–3.3 μm [9]–[12]. Limited research has been conducted on edge couplers optimally designed for input light sources with non-circular incident beams, such as the elliptic beams from distributed feedback (DFB) lasers. The DFB lasers have been widely used as laser sources for optical communication systems and high bitrate interconnects in data center networks due to the superior characteristics of extremely narrow optical linewidth and great temperature stability [13]–[15]. However, a DFB laser usually features an elliptical beam profile because the emission aperture is not circular. As a result, the coupling of its light into an optical fiber requires additional anamorphic lens [16] which may increases the difficulty and cost of packaging for small form-factor pluggable (SFP) transceiver modules. Direct edge coupling of the DFB laser beam into silicon photonic circuits without the use of lensed fiber can bypass this problem and its small footprint is beneficial to SFP transceiver modules. Hence, designing a highly efficient edge coupler for directly coupling the DFB laser into silicon photonic circuits is crucial in practical applications.

In this study, we design a high-efficiency ultra-broadband multi-tip edge coupler based on the SOI platform for directly coupling a DFB laser which emits an elliptical beam profile into silicon photonic circuits. The benefits of using the multi-tip edge coupler are twofold. First, the mode profile at the entrance side of the multi-tip edge coupler can be easily designed to match the field profile of the elliptical beam emitted from the DFB laser to minimize the mode mismatch loss. Second, the multi-tip edge coupler can be optimized only for TE mode coupling without the concern of polarization dependent loss. Because the light emitted from DFB lasers is typically polarized in the direction parallel to the epitaxial layer interface, it only excites the TE modes in the SOI waveguide. Section 2 describes the proposed device structure. The designed structure consists of a multi-tip section followed by a combiner section with the waveguide and gap width at least as large as the minimum allowable value (150 nm in this study, e.g., imec iSiPP50G) for a practical fabrication process. This structure can be simply fabricated by one step etching on SOI platform. In Section 2.1, the coupling efficiencies of the multi-tip edge couplers with a varying number of tips are analyzed first. The particle swarm optimization (PSO) method [17], [18] was used to optimize the widths of the tips and the spacing between tips to match the mode field of the multi-tip edge coupler with the output mode of the DFB laser at the input interface. The input interface coupling efficiency is calculated as the fitness function for the PSO by using the finite difference eigenmode (FDE) technique [19]. Section 2.2 describes the determination of the structural parameters with inclusion of the taper and device footprint in the coupling efficiency via the eigenmode expansion (EME) method [20], for the reduction of the loss during mode evolution. Furthermore, an offset region is proposed to reduce

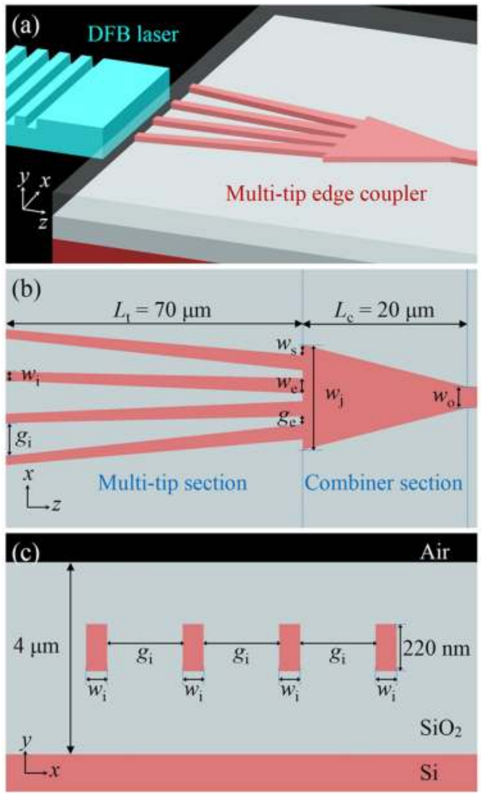

Fig. 1. Schematic layout of the proposed multi-tip edge coupler: (a) 3D, (b) top, and (c) cross-sectional views of the four-tip edge coupler.

the mode mismatch caused by the structural discontinuity. In Section 3, the determination of the overall coupling efficiency using the three-dimensional finite-difference time-domain (3-D FDTD) technique [21]–[23] is described. For practical applications, the tolerances against the misalignment of the light source and the fabrication error of the edge couplers are also calculated and discussed.

2. Design of Multi-Tip Edge Couplers

The schematic of the multi-tip edge couplers is shown in Fig. 1. The proposed devices are channel waveguides on the SOI platform with a 2-μm-thick buried oxide layer and a 220-nm-thick device silicon layer. The channel waveguides are covered with a 2-μm-thick top cladding silicon dioxide layer. The devices are composed of a multi-tip section and a combiner section. The multi-tip section is composed of a number (N) of equally spaced inverse taper waveguides. The width of each inverse taper waveguide linearly increases from an initial width of w_i to an exit width of w_e and each gap width between inverse taper waveguides linearly decreases from an initial gap width of g_i to an exit gap width of g_e, thus enabling low-loss mode evolution. The combiner section, which connects the multi-tip section and the output channel waveguide, is an adiabatic taper waveguide with its width linearly decreasing from an initial width of w_j at the junction between two sections to a final width of w_o to match the output channel waveguide. These geometric parameters are limited to be larger than the minimum feasible waveguide width and gap width allowed for the fabrication process, 150 nm, with this value selected to be representative of typical foundry services.

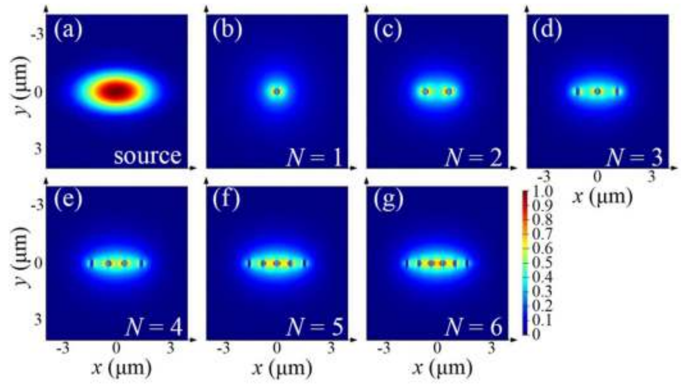

Fig. 2. Normalized electric field distributions of the fundamental TE modes at 1550 nm for (a) the DFB laser, (b) the conventional inverse taper edge coupler (labeled as $N = 1$), and (c)–(g) the multi-tip edge couplers for $N = 2$–6, respectively, at the input interface.

2.1 Choice of Number of Tips

In this study, the light source was a DFB laser with linear TE polarization, centered at 1550 nm with an elliptic Gaussian field profile. This profile had a $1/e$ half width of 1.62 μm in the x-axis, σ_x, and a $1/e$ half height of 0.87 μm in the y-axis, σ_y, as shown in Fig. 2(a). The overall coupling efficiency, η_c, of the multi-tip coupler can be calculated as

$$\eta_c = \eta_i \times \eta_m$$

where the input interface coupling efficiency, η_i, is determined by how well the modes match each other, while the mode evolution efficiency, η_m, is determined by how well the mode evolves adiabatically. In order to obtain the highest η_i between the output mode of the DFB laser and the mode field of the multi-tip edge couplers at the input interface, the values of N, w_i, and g_i were optimized using the PSO method. This optimization was carried out as follows:(*i*) The fundamental TE mode profile of the DFB laser and the fundamental TE mode field of the multi-tip edge couplers with certain values of tip widths w_i and gaps g_i at the input interface are calculated by using the FDE technique. Then, (*ii*) η_i is determined by using the mode overlap integral as well as the reflection caused by the difference between the effective indices at the two sides of the input interface [24]. Lastly, (*iii*) the calculated η_i is used as the fitness value for the PSO to iterate through steps (*i*) and (*ii*) to obtain the optimized tip widths w_i and gaps g_i at the input interface for the configurations with different number of tips.

The mode profile of the fundamental TE mode at 1550 nm at the input interface of the inverse taper edge coupler with the optimized tip width and $N = 1$, which is the conventional inverse taper edge coupler, is presented in Fig. 2(b). The normalized electric field distributions of the fundamental TE modes at 1550 nm at the input interface of the multi-tip edge couplers with different number of tips ($N = 2$–6) as well as their respective optimized tip widths w_i and gaps g_i are shown in Fig. 2(c)–(g), respectively. η_i for each configuration is shown in Fig. 3. The single-tip edge coupler ($N = 1$) has an input interface coupling efficiency of $\eta_i = 84.50\%$, in contrast to the increased efficiency of the multi-tip edge couplers, which exceeds 91.78% for $N = 2$–6. The peak η_i of 94.70% is at $N = 4$, which is $\sim$10% higher than that of the conventional inverse taper edge coupler. The optimized tip widths, gaps, and resulting input interface coupling efficiencies are shown in Table 1. Fig. 3 shows that η_i for $N = 5$ is comparable with that for $N = 4$. However, as indicated by Table 1, the lower tip numbers (for $N = 2$–6) have greater tip widths w_i and gaps g_i, and thus considering that the manufacturability and fabrication tolerances are improved with larger w_i and g_i, $N = 4$ is a better choice than $N = 5$ owing to its larger widths and gaps yet similar input interface efficiency. Therefore, the following discussion is mainly focused on $N = 4$. Once the optimized tip widths w_i

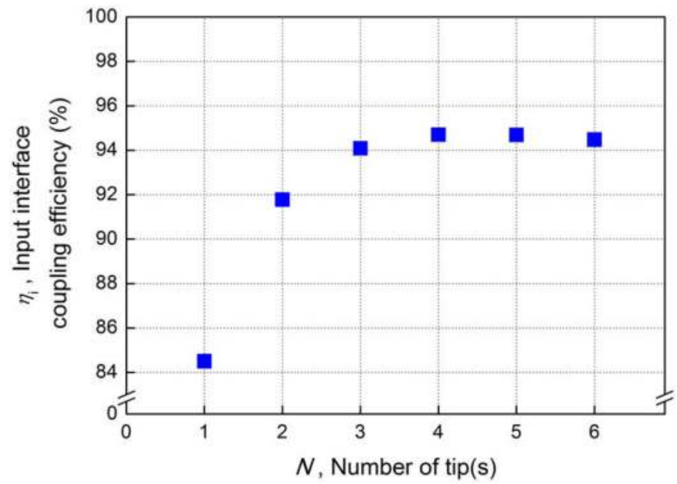

Fig. 3. Input interface coupling efficiency η_i between the DFB laser and multi-tip edge couplers with different number (N) of tips at 1550 nm. Note that the data at $N = 1$ indicates the value of η_i for the conventional inverse taper edge coupler.

TABLE 1

Optimized Parameters (w_i and g_i) and the Calculated Input Interface Coupling Efficiency, η_i, for $N =$ 1–6. Note That the Data at $N = 1$ Indicate the Optimized Parameters and η_i for the Conventional Inverse Taper Edge Coupler

N	1	2	3	4	5	6
g_i (nm)	–	990	785	639	518	438
w_i (nm)	182	186	183	177	165	154
η_i (%)	84.50	91.78	94.09	94.70	94.69	94.48

and gaps g_i for each N are determined, the mode evolution efficiency η_m for the given parameters can be further analyzed, which is described in the next section.

To explore how the η_i changes with the parameters g_i and w_i around their optimized values, we carried out an additional calculation of η_i with the parameters $w_i = 150$–200 nm and $g_i = 613$–663 nm for the multi-tip edge coupler $N = 4$ at 1550 nm. The mapping of η_i for w_i and g_i is shown in Fig. 4. The result shows that η_i is more sensitive to w_i than g_i.

2.2 Design of Adiabatic Tapers

The mode evolution efficiency η_m is affected by the structural discontinuity at the junction of the multi-tip section and combiner section as well as the adiabaticity of the tapers in both sections. This structural discontinuity results from a limitation of the fabrication process that creates an inevitable gap width g_e at the junction between the two sections, thus causing an additional mode mismatch. To reduce this mode mismatch, we propose an extra width offset region w_s of the combiner section at the junction of the multi-tip section and combiner section, where $w_j = (N - 1) \times g_e + N \times w_e + 2w_s$. The optimization of parameters w_e, g_e, and w_s for these two sections is carried out by the same method described previously. All of the optimized parameters for $N = 1$–6 are shown in Table 2. The optimized parameters for $N = 4$ are $w_e = 294$ nm, $g_e = 150$ nm, and $w_s = 206$ nm, and thus $w_j = 2038$ nm. These parameters are applied to the EME and the 3D-FDTD simulations for the following discussion.

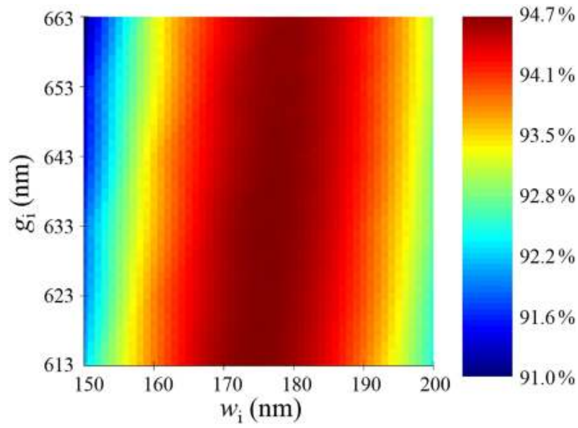

Fig. 4. The Input interface coupling efficiency η_i as a function of w_i = 150–200 nm and g_i = 613–663 nm for the multi-tip edge coupler with $N = 4$ at 1550 nm.

TABLE 2

Optimized Parameters (w_e and w_s) for $N = 1$–6. Note that the Data at $N = 1$ Indicate the Optimized Parameters for the Conventional Inverse Taper Edge Coupler

N	1	2	3	4	5	6
w_e (nm)	400	297	295	294	292	295
w_s (nm)	–	225	210	206	195	197

Ideally, adiabaticity of the tapers in both the multi-tip section and the combiner section can be achieved as the lengths of the tapers become infinitely large. While a device with a small footprint and high mode evolution efficiency η_m is desirable, there is a trade-off between increasing η_m and maintaining a small device footprint. For the analysis of the adiabaticity of the tapers, the overall coupling efficiency η_c is calculated by using the EME technique instead of the time-consuming 3-D FDTD technique as the redundant calculations of mode evolutions in tapers with variable lengths can be eliminated and thus the calculation time can be significant shortened [20]. The variations of the overall coupling efficiency η_c of the multi-tip edge coupler as a function of the multi-tip section length L_t and combiner section length L_c are shown in Fig. 5(a) and (b), respectively. To maintain a small device footprint, section lengths of $L_t = 70$ μm and $L_c = 20$ μm were selected for the device geometries with $N = 1$–6.

3. Results and Discussion

3-D FDTD simulations were used to determine more accurate overall coupling efficiencies η_c of the multi-tip edge couplers with $N = 1$–6 the results are presented in Fig. 6. The variation of η_c with N is similar to that of the input interface coupling efficiency η_i (see Fig. 3). For the multi-tip edge couplers with $N = 2$–6, the mode evolution efficiency $\eta_m = \eta_c / \eta_i$ is approximately 0.95, which indicates that the lengths for the tapers are sufficiently large to allow adiabatic mode evolution for all the multi-tip edge couplers. Among the proposed devices with different number of tips, the four-tip edge coupler has the highest overall coupling efficiency η_c at 90.68% (0.4249 dB), which is ~10% higher than that of the conventional inverse taper edge coupler (η_c = 82.66% or 0.8272 dB). The cross-sectional view at $y = 0$ of the simulated electric field incident from a DFB laser at 1550 nm into the 90-μm-long four-tip edge coupler is shown in Fig. 7. The mode field evolves smoothly and

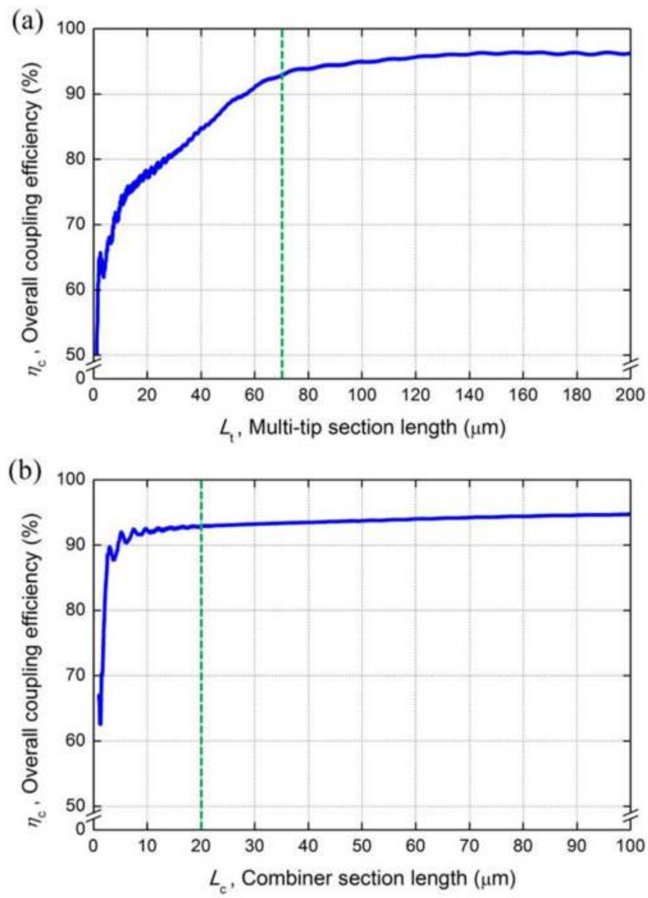

Fig. 5. Overall coupling efficiency η_c of the four-tip ($N = 4$) edge coupler determined via the EME method at 1550 nm with different (a) multi-tip section lengths L_t (with fixed $L_c = 20$ μm) and (b) combiner section lengths L_c (with fixed $L_t = 70$ μm). The green dotted lines indicate the parameters we choose for the following 3-D FDTD simulations.

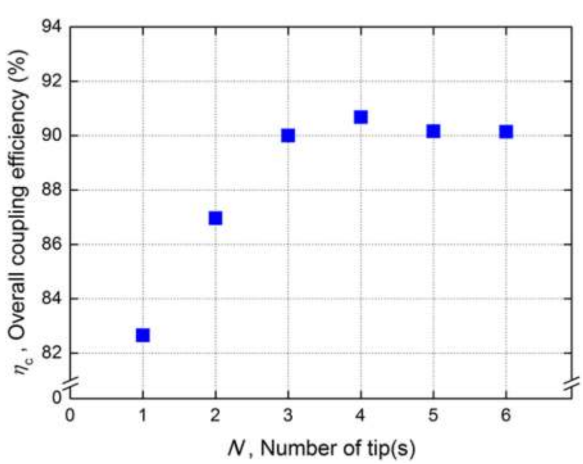

Fig. 6. Overall coupling efficiency η_c as calculated by the 3-D FDTD method, of the multi-tip edge coupler with different number of tips N at 1550 nm. Note that the data at $N = 1$ indicates the η_c of the conventional inverse taper edge coupler.

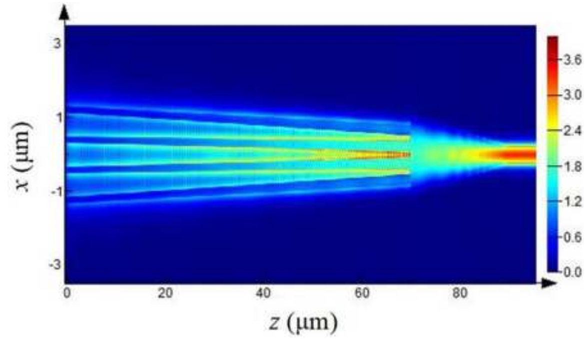

Fig. 7. Mode propagation of the 90-μm-long four-tip edge coupler at 1550 nm from the 3-D FDTD simulation.

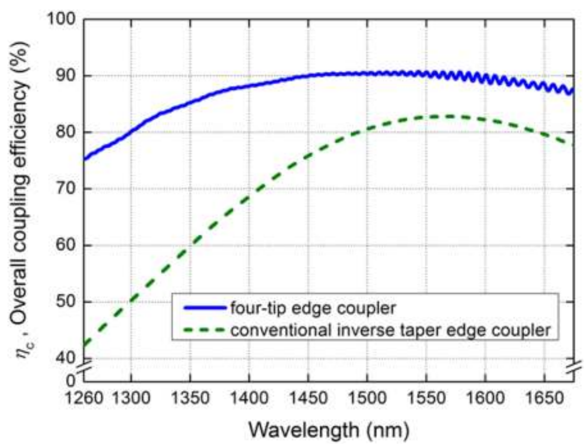

Fig. 8. Overall coupling efficiency η_c as a function of incident wavelengths 1260–1675 nm calculated by 3-D FDTD simulations for the four-tip edge coupler and the conventional inverse taper edge coupler.

gradually from the mode size of the light source ($\sigma_x = 1.62\ \mu$m and $\sigma_y = 0.87\ \mu$m) to the mode size in the 400-nm-wide and 220-nm-thick output channel waveguide without noticeable loss.

The overall coupling efficiencies η_c as a function of incident wavelengths 1260–1675 nm for the four-tip edge coupler is shown in Fig. 8. The minimum η_c of 75.19% (1.238 dB) and the ultra-broadband operation over 415 nm, across the O-band to U-band, can be achieved. The four-tip edge coupler shows higher efficiency and much broader bandwidth than the conventional inverse taper edge coupler. It is noted that there is a slight oscillation characteristics of the overall coupling efficiency for the four-tip edge coupler. This is originated from the Fabry-Pérot resonance between the end faces of the multi-tip edge coupler. On the other hand, since the conventional coupler is simply a single inverse taper waveguide structure without an abrupt structural change at the joint between the taper waveguide and the output waveguide to provide a required reflection to form a Fabry-Pérot cavity. Therefore, there is no oscillation behavior of the overall coupling efficiency for the conventional coupler.

Figure 9 shows the mode profile of the source and the field distribution of the multi-tip edge couplers for $N = 1$ and $N = 4$ at three different wavelengths, i.e., 1260 nm, 1550 nm, and 1660 nm, to further explicate the spectral characteristics of the input interface coupling efficiency η_{fi}. The mode field distribution area for $N = 1$ decreases dramatically at shorter wavelengths while the mode field distribution area for $N = 4$ shows less variation. Based on the calculations of η_{fi}, the value of η_{fi} for $N = 1$ is decreased from 84.5% at 1550 nm to 43.5% at 1260 nm while the value of η_{fi} for $N = 4$ is decreased from 94.7% at 1550 nm to 75.4% at 1260 nm. Within this wavelength range, the η_{fi}

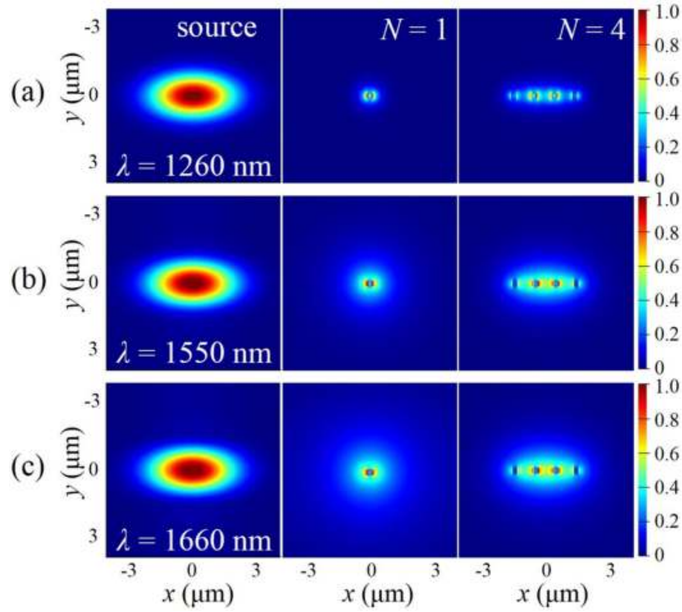

Fig. 9. Normalized electric field distributions of the fundamental TE modes at the input interface for the DFB laser, the conventional inverse taper edge coupler (labeled as $N = 1$), and the four-tip edge coupler (labeled as $N = 4$), at (a) 1260 nm, (b) 1550 nm, and (c) 1660 nm, respectively.

for $N = 4$ is reduced less than that for $N = 1$ as the wavelength deviates from the target central wavelength 1550 nm. Consequently, the bandwidth for the four-tip edge coupler ($N = 4$) is wider than that for the conventional inverse-taper edge coupler ($N = 1$).

The overall coupling loss l_c, where $l_c = -10 \cdot \log(\eta_c)$ (in dB), for both the four-tip edge coupler and the conventional inverse taper edge coupler as functions of the misalignment of the light source in the *x*-axis and the *y*-axis are shown in Fig. 10(a) and (b), respectively. The misalignment tolerance of the four-tip edge couplers for a 1 dB loss penalty is ± 0.77 μm in the horizontal direction (*x*-axis), which is 10% higher than the conventional inverse taper edge coupler. For the vertical direction (*y*-axis), the misalignment tolerance for a 1 dB loss penalty is ± 0.41 μm. Such misalignment tolerances in both horizontal and vertical directions are easily achievable by the modern alignment technique.

We also investigated the tolerance of a fabrication error Δw of ± 5 nm and ± 10 nm in variations of the feature sizes. In this study, isotropic variations of the feature sizes in both *x*-axis and *y*-axis directions were considered. The plus sign (+) indicates that the feature size is larger than the designed size, whereas the minus sign (–) indicates that the feature size is smaller than the designed size. In Fig. 11, the four-tip edge coupler shows extra losses of only 0.0262 dB for $\Delta w = -5$ nm and 0.0617 dB for $\Delta w = -10$ nm, indicating that the designed device is tolerant to fabrication errors. Notably, the overall coupling efficiency for both $\Delta w = +5$ nm and $+10$ nm was higher than that for $\Delta w = 0$. This is because g_e for $\Delta w = +5$ nm and $+10$ nm is less than the minimum feasible gap width as limited by the fabrication process, thus further reducing the structural discontinuity between the multi-tip section and the combiner section resulting in less mode evolution loss. With advances in the fabrication technology in the future resulting in smaller minimum feasible widths, a higher overall coupling efficiency η_c can be expected. In the ideal case that the minimum feasible gap width is zero, the highest overall coupling efficiency $\eta_c = 94.06\%$ (0.2659 dB) can be achieved according to our calculations. The comparisons of the performances of the proposed device with various state-of-the-art multi-tip edge couplers on SOI platform are shown in Table 3. The performance of the proposed device is comparable with the other state-of-the-art multi-tip edge

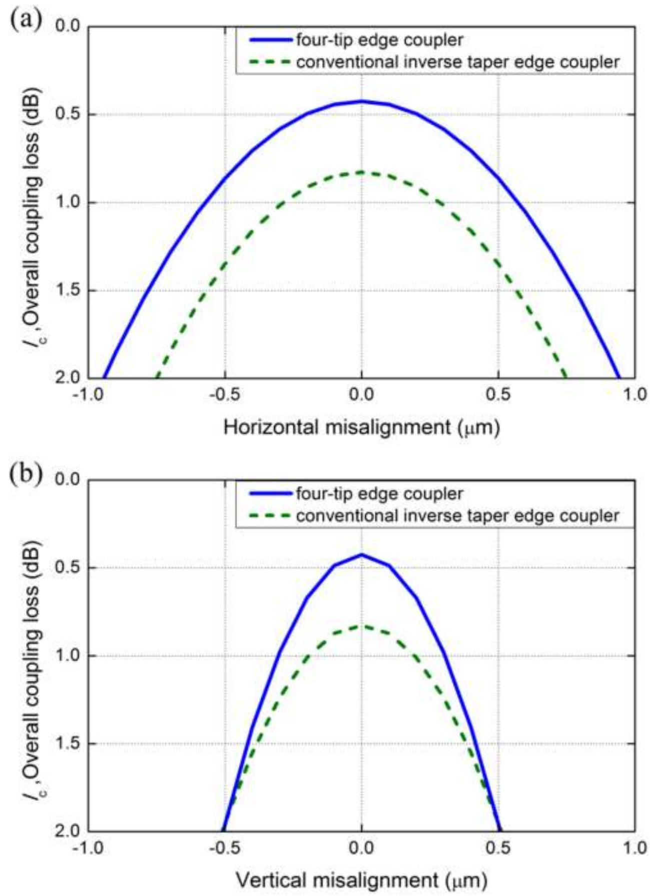

Fig. 10. Overall coupling loss l_c for both the four-tip edge coupler and the conventional inverse taper edge coupler as functions of the misalignment of the light source in the (a) horizontal (*x*-axis) and (b) vertical (*y*-axis) directions calculated by the 3-D FDTD method at a wavelength of 1550 nm.

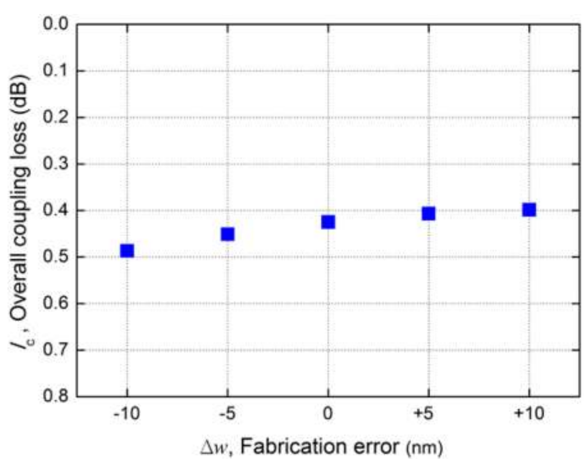

Fig. 11. Calculated overall coupling loss l_c for the four-tip edge coupler as functions of fabrication error Δw, for $\Delta w = \pm 5$ and ± 10 nm.

TABLE 3
Comparison of Various Designs of Multi-Tip Edge Couplers on SOI Platform at 1550 nm

<table>
<tr><th rowspan="2"># of tips & structure [Ref.]</th><th rowspan="2">Source & MFD (μm)</th><th rowspan="2">Total length (μm)</th><th colspan="2">Overall insertion loss (dB)</th><th rowspan="2">Bandwidth (nm)</th><th rowspan="2">Minimum line/gap widths (nm)</th></tr>
<tr><th>Simulation (sim.)</th><th>Experiment (exp.)</th></tr>
<tr><td>2-tips to 1-MMI [9]</td><td>lensed fiber 3.3</td><td>40</td><td>0.55 (approx.) (TE) 1.35 (approx.) (TM)</td><td>1.10 (TE) 1.52 (TM)</td><td>150 (0.3-dB BW) (1480–1630) (exp.)</td><td>140</td></tr>
<tr><td rowspan="2">2-tips to 1-waveguide (Trident) [10]</td><td>lensed fiber 3</td><td rowspan="2">150</td><td>0.34 (TE) 0.62 (TM)</td><td>0.92 (TE) 0.94 (TM)</td><td rowspan="2">NA</td><td rowspan="2">100</td></tr>
<tr><td>Fabry–Pérot laser diode 3</td><td>NA</td><td>2.3 (TE)</td></tr>
<tr><td>2-tips to 2-waveguides (separately)</td><td rowspan="2">Fabry–Pérot laser diode 2.46 × 2.2</td><td>96</td><td>1.42 (TE)</td><td>2 (TE)</td><td>60 (1-dB BW) (exp.)</td><td>180</td></tr>
<tr><td>5-tips to 1-MMI [11]</td><td>156.7</td><td>2.2 (TE)</td><td>3.1 (TE)</td><td>28 (1-dB BW) (exp.)</td><td>180</td></tr>
<tr><td>3-tips to 1-taper [12]</td><td>Lensed fiber 2.5</td><td>137.45 (sim.) 101 (exp.)</td><td>0.27 (TE)</td><td>1.8 (TE & TM)</td><td>80 (0.5-dB BW) (1520–1600) (exp.)</td><td>120</td></tr>
<tr><td>4-tips to 1-taper (this work)</td><td>DFB laser 3.24 × 1.74</td><td>90</td><td>0.42 (TE) (sim.)</td><td>NA</td><td>> 415 (1-dB BW) (1260–1675) (sim.)</td><td>150</td></tr>
</table>

couplers in terms of overall insertion loss and total device length. Especially, the proposed device exhibits an extraordinary broad bandwidth of at least 415 nm.

The aforementioned design process is not limited to be applied to the cases discussed in this study. For a more general case, when the ellipticity of source differs or the size ratios between the waveguide height and the spot size of source varies, one can first optimize the tip number and tip geometry at the input surface with considering the minimum allowable value for parameters (w_i and g_i). It can be expected that, the small mode field distribution for $N = 1$ causes a small overlapping area between the field distribution at input interface and the mode profile of the source leading to the lowest η_i. By introducing additional number of tips, the overlapping area can be further increased and thus the value of η_i increases accordingly. Nevertheless, when the number of tips exceeds a certain value N_{max} (e.g., $N = 4$ in this study), the field distribution becomes similar and large enough to well match the mode profile of the source and hence η_i cannot be further enhanced. It should be noted that we restrict the optimized value of the parameter w_i to be at least as large as the minimum allowable value (e.g., 150 nm in this study for imec iSiPP50G foundry service) for a practical fabrication process. As a result, the value of η_i for $N > N_{max}$ may be limited or even decreased due to the tip width or gap width reaching their minimum allowable values. As the parameters w_i and g_i for the case with $N = N_{max}$ are determined, then the parameters (w_e and w_s) of the tip geometry at the joint between the multi-tip section and the combiner section can be optimized using the same mode matching concept. Finally, the overall coupling efficiency dependence on L_t and L_c can be determined by carrying out EME simulations and then the optimized values of L_t and L_c can be chosen based on the trade-off between increasing η_m and maintaining a smaller device footprint.

4. Conclusions

In summary, high efficiency and ultra-broadband multi-tip edge couplers based on the SOI platform for direct coupling with the elliptic beam of a DFB lasers were developed. The devices are composed of a multi-tip section and a combiner section with dimensions not less than the minimum allowed waveguide width and gap for the practical fabrication process. To obtain the best mode matching at the input interface between the DFB laser and the multi-tip section, the width and the spacing of tips were optimized by using the PSO method with the number of tips varied from one to six. The highest input interface coupling efficiency of 94.70% was found for the four-tip edge coupler. Given the trade-off between the adiabaticity of the tapers and the small device footprint, lengths of 70 μm and 20 μm were chosen for the taper structures in the multi-tip section and the combiner section, respectively. Moreover, an extra width offset region of the combiner section was introduced at the junction of the multi-tip section and combiner section to reduce the mode mismatch caused by the structural discontinuity at this junction. For the four-tip edge coupler, an overall coupling efficiency of up to 90.68% (0.4249 dB) at 1550 nm with ultra-broadband operation from 1260 nm to 1675 nm with less than 1 dB extra loss was verified by the 3-D FDTD technique. The misalignment tolerance of the four-tip edge coupler for the 1 dB loss penalty is $\pm$0.77 μm in the horizontal direction (x-axis) and $\pm$0.41 μm in the vertical direction (y-axis), which are compatible with the modern alignment technique. With advancements in fabrication technologies that allow for smaller minimum feasible widths and gaps in the future, an even higher overall coupling efficiency is anticipated. With its high-efficiency ultra-broadband operation and small device footprint, the proposed device is a promising candidate for a laser-to-chip edge coupler in silicon photonics.

References

[1] L. Liu and Z. Zhou, "Refractive index engineering of high performance coupler for compact photonic integrated circuits," *Jpn. J. Appl. Phys.*, vol. 56, no. 4S, Apr. 2017, Art. no. 04CA01, doi: 10.7567/JJAP.56.04CA01.
[2] C. R. Doerr *et al.*, "Monolithic polarization and phase diversity coherent receiver in silicon," *J. Lightw. Technol.*, vol. 28, no. 4, pp. 520–525, Feb. 2010, doi: 10.1109/JLT.2009.2028656.
[3] P. Dumon *et al.*, "Compact wavelength router based on a Silicon-on-insulator arrayed waveguide grating pigtailed to a fiber array," *Opt. Exp.*, vol. 14, no. 2, pp. 664–669, Jan. 2006, doi: 10.1364/OPEX.14.000664.
[4] L. Yu, L. Liu, Z. Zhou, and X. Wang, "High efficiency binary blazed grating coupler for perfectly-vertical and near-vertical coupling in chip level optical interconnections," *Opt. Commun.*, vol. 355, no. 15, pp. 161–166, Nov. 2015, doi: 10.1016/j.optcom.2015.06.003.
[5] D. Vermeulen *et al.*, "High-efficiency fiber-to-chip grating couplers realized using an advanced CMOS-compatible silicon-on-insulator platform," *Opt. Exp.*, vol. 18, no. 17, pp. 18278–18283, Aug. 2010, doi: 10.1364/OE.18.018278.
[6] D. Taillaert *et al.*, "Grating couplers for coupling between optical fibers and nanophotonic waveguides," *Jpn. J. Appl. Phys.*, vol. 45, no. 8A, pp. 6071–6077, Aug. 2006, doi: 10.1143/JJAP.45.6071.
[7] L. Chen, C. R. Doerr, Y. K. Chen, and T. Y. Liow, "Low-loss and broadband cantilever couplers between standard cleaved fibers and high-index-contrast Si_3N_4 or Si waveguides," *IEEE Photon. Technol. Lett.*, vol. 22, no. 23, pp. 1744–1746, Dec. 2010, doi: 10.1109/LPT.2010.2085040.
[8] V. R. Almeida, R. R. Panepucci, and M. Lipson, "Nanotaper for compact mode conversion," *Opt. Lett.* vol. 28, no. 15, pp. 1302–1304, Aug. 2003, doi: 10.1364/OL.28.001302.
[9] J. Wang *et al.*, "Low-loss and misalignment-tolerant fiber-to-chip edge coupler based on double-tip inverse tapers," in *Proc. Opt. Fiber Commun. Conf. Exhib.*, Anaheim, CA, USA, Mar. 2016, Paper M2I.6, doi: 10.1364/OFC.2016.M2I.6.
[10] N. Hatori *et al.*, "A hybrid integrated light source on a silicon platform using a trident spot-size converter," *J. Lightw. Technol.*, vol. 32, no. 7, pp. 1329–1336, Apr. 2014, doi: 10.1109/JLT.2014.2304305.
[11] S. Romero-García, B. Marzban, F. Merget, B. Shen, and J. Witzens, "Edge couplers with relaxed alignment tolerance for pick-and-place hybrid integration of III-V lasers with SOI waveguides," *IEEE J. Sel. Topics Quantum Electron.*, vol. 20, no. 4, pp. 369–379, Jul./Aug. 2014, Art. no. 8200611, doi: 10.1109/JSTQE.2013.2292523.
[12] K. Han, M. Teng, B. Niu, Y. Lee, S. Kim, and M. Qi, "Double slot fiber-to-chip coupler using direct strip-slot mode coupling," in *Proc. Opt. Fiber Commun. Conf. Exhib.*, Los Angeles, CA, USA, Mar. 2017, Paper Th2A.1, doi: 10.1364/OFC.2017.Th2A.1.
[13] W. Kobayashi *et al.*, "Design and fabrication of 10-/40-Gb/s, uncooled electroabsorption modulator integrated DFB laser with butt-joint structure," *J. Lightw. Technol.*, vol. 28, no. 1, pp. 164–171, Jan. 2010, doi: 10.1109/JLT.2009.2036865.
[14] J. Hauck *et al.*, "Stabilization and frequency control of a DFB laser with a tunable optical reflector integrated in a silicon photonics PIC," *J. Lightw. Technol.*, vol. 34, no. 23, pp. 5467–5473, Dec. 2016, doi: 10.1109/JLT.2016.2616947.
[15] S. Dhoore, A. Koninger, R. Meyer, G. Roelkens, and G. Morthier, "Electronically tunable distributed feedback (DFB) laser on silicon," *Laser Photon. Rev.*, vol. 13, no. 3, Mar. 2019, Art. no. 1800287, doi: 10.1002/lpor.201800287.
[16] R. A. Modavis and T. W. Webb, "Anamorphic microlens for laser diode to single-mode fiber coupling," *IEEE Photon. Technol. Lett.*, vol. 7, no. 7, pp. 798–800, Jul. 1995, doi: 10.1109/68.393210.

[17] J. Robinson and Y. Rahmat-Samii, “Particle swarm optimization in Electromagnetics,” *IEEE Trans. Antennas Propag.*, vol. 52, no. 2, pp. 397–407, Feb. 2004, doi: 10.1109/TAP.2004.823969.
[18] K. E. Parsopoulo and M. N. Vrahatis, *Particle Swarm Optimization and Intelligence: Advances and Applications*. Hershey, PA, USA: Information Science Reference, 2010.
[19] Z. Zhu and T. Brown, “Full-vectorial finite-difference analysis of microstructured optical fibers,” *Opt. Exp.*, vol. 10, no. 17, pp. 853–864, Aug. 2002, doi: 10.1364/OE.10.000853.
[20] G. V. Eleftheriades, A. S. Omar, L. P. B. Katehi, and G. M. Rebeiz, “Some important properties of waveguide junction generalized scattering matrices in the context of the mode matching technique,” *IEEE Trans. Microw. Theory Techn.* vol. 42, no. 10, pp. 1896–1903, Oct. 1994, doi: 10.1109/22.320771.
[21] D. M. Sullivan, *Electromagnetic Simulation Using the FDTD Method*. New York, NY, USA: IEEE Press, 2000.
[22] A. Taflove and S. C. Hagness, *Computational Electromagnetics: The Finite-Difference Time-Domain Method*. Boston, MA, USA: Artech House, 2005.
[23] S. D. Gedney, *Introduction to the Finite-Difference Time-Domain (FDTD) Method for Electromagnetics*. Fort Collins, CO, USA: Morgan & Claypool, 2011.
[24] A. W. Snyder and J. Love, *Optical Waveguide Theory*. London, U.K.: Chapman & Hall, 1983.